PROCEEDINGS, 43rd Workshop on Geothermal Reservoir Engineering
Stanford University, Stanford, California, February 12-14, 2018
SGP-TR-213

Numerical Modeling of High Energy Geothermal Systems with Soil Atmosphere Boundary Condition

Laurence BEAUDE, Konstantin BRENNER, Simon LOPEZ, Roland MASSON, Farid SMAI

LJAD, Université Côte d'Azur, CNRS, INRIA COFFEE, LJAD - Parc Valrose, 06108 Nice cedex 2, France

laurence.beaude@unice.fr

Keywords: non-isothermal compositional Darcy flow, geothermal energy, soil-atmosphere boundary condition, outflow boundary condition, porous medium drying, finite volume scheme.

ABSTRACT

This article deals with the modeling and formulation of compositional gas liquid Darcy flow. Our model includes an advanced boundary condition at the interface between the porous medium and the atmosphere accounting for convective mass and energy transfer, liquid evaporation and liquid outflow. The formulation is based on a fixed set of unknowns whatever the set of present phases. The thermodynamic equilibrium is expressed as complementary constraints. The model and its formulation are applied to the simulation of the Bouillante high-energy geothermal field in Guadeloupe characterized by a high temperature closed to the surface.

1. INTRODUCTION

Taking into account water table fluctuations and the interaction of shallow water levels with geothermal systems while modeling their natural state is notoriously difficult. We investigate a new formulation for the non-isothermal compositional gas liquid Darcy flows and its coupling with an advanced soil-atmosphere boundary condition.

The latest is needed to model the soil-atmosphere interaction because the coupling between the porous medium and surface flows would not be computationally realistic for geothermal time and space scales. This soil-atmosphere boundary condition is based on mole and energy balance equations expressed at the interface, taking into account the vaporization of the liquid phase in the atmosphere, the convective molar and energy transfer, a liquid outflow condition as well as the precipitation and radiation terms. The compositional model typically accounts for the water component that can vaporize into the gas phase and a set of gaseous components which can dissolve in the liquid phase (air…).

Then, we choose a formulation that is based on the pressures, saturations, temperature and phase molar fractions as set of unknowns. No switch of variables is required as this choice of unknowns is combined with an extension of the phase molar fractions of an absent phase by the molar fractions at thermodynamic equilibrium with the present phase. This implies that the set of unknowns does not depend on the set of present phases. More precisely, the phase transitions are expressed as complementary constraints which results that the non-linear system can be solved using semi-smoothed Newton algorithms.

The model and its formulation are applied on the Bouillante high temperature geothermal field located in Guadeloupe which show temperature of 250°C around 300m deep and soil with near boiling conditions in some places.

2. NON-ISOTHERMAL COMPOSITIONAL TWO-PHASE DARCY FLOW MODEL

We consider a non-isothermal compositional liquid gas Darcy flow model with $\{g,l\}$ denoting the set of gas and liquid phases. Each phase $\alpha \in \{g,l\}$ is a mixture of a set of components denoted by C including typically a water component, denoted w, which can vaporize in the gas phase and a set of gaseous components that can dissolve in the liquid phase. The thermodynamic properties of each phase $\alpha \in \{g,l\}$ depend on its pressure P^α, the local equilibrium temperature of the system T and its molar fractions $C^\alpha = (C_i^\alpha)_{i\in C}$.

For each phase $\alpha \in \{g,l\}$, we denote by $\zeta^\alpha(\mathrm{P}^\alpha, T, C^\alpha)$ its molar density, by $\rho^\alpha(\mathrm{P}^\alpha, T, C^\alpha)$ its mass density, by $\mu^\alpha(\mathrm{P}^\alpha, T, C^\alpha)$ its dynamic viscosity, by $\mathrm{e}^\alpha(\mathrm{P}^\alpha, T, C^\alpha)$ its molar internal energy and by $\mathrm{h}^\alpha(\mathrm{P}^\alpha, T, C^\alpha)$ its molar enthalpy. For the gas phase, as we consider an ideal gas mixture, the molar enthalpy is defined by

$$h^g(P^g, T, C^g) = \sum_{i\in C} C_i^g \; h_i^g(P^g, T), \tag{1}$$

where $\mathrm{h}_\mathrm{i}^\mathrm{g}(\mathrm{P}^g, T)$ is the molar enthalpy of the component i in the gas phase.

Thermodynamic equilibrium between the gas and liquid phases will be assumed for each component and governed by the phase fugacities denoted by $\mathrm{f}^\alpha(\mathrm{P}^\alpha, T, C^\alpha) = (f_i^\alpha(\mathrm{P}^\alpha, T, C^\alpha))_{i\in C}$, $\alpha \in \{g,l\}$. The rock porosity is denoted by $\phi(\boldsymbol{x})$ and the rock permeability tensor by $\boldsymbol{\Lambda}(\boldsymbol{x})$ where $\boldsymbol{x}$ denotes the spatial coordinates. The hydrodynamic Darcy laws are characterized by the relative permeability $k_r^\alpha(\boldsymbol{x}, S^\alpha)$ of each phase $\alpha \in \{g,l\}$, as a function of the phase saturation S^α, and by the capillary pressure $P_c(\boldsymbol{x}, S^\alpha) = P^g - P^l$. The

dependence of the relative permeabilities and capillary pressure on $\boldsymbol{x}$, which is piecewise constant for each rocktype, is omitted in the following for the sake of simplicity.

Our formulation of the model is based on the fixed set of unknowns defined by

$$X = (P^\alpha, T, S^\alpha, C^\alpha, \alpha \in \{\mathrm{g}, \mathrm{l}\}). \tag{2}$$

Note that, as opposed to the Coats' variable switch formulation (see Class, Helmig and Bastian (2002)), the molar fractions C^α of an absent phase α are extended by the ones at equilibrium with the present phase in the sense that the equality of the gas and liquid fugacities always holds $\mathrm{f}^g(\mathrm{P}^g, T, C^g) = \mathrm{f}^l(\mathrm{P}^l, T, C^l)$. Let $n_i(X)$ be the number of moles of the component $\mathrm{i} \in \mathrm{C}$ per unit pore volume defined by

$$n_i(X) = \sum_{\alpha \in \{\mathrm{g}, \mathrm{l}\}} \xi^\alpha S^\alpha C_i^\alpha, \quad i \in C. \tag{3}$$

We introduce the rock energy per unit rock volume defined by $E_r(T)$ and the fluid energy per unit pore volume defined by $E(X) = \sum_{\alpha \in \{g,l\}} \zeta^\alpha \mathrm{S}^\alpha e^\alpha$. Let us denote by $\mathbf{g}$ the gravitational acceleration vector. The generalized Darcy velocity of the phase $\alpha \in \{g, l\}$ is given by

$$V^\alpha = -\frac{k_r^\alpha}{\mu^\alpha} \Lambda(x) \left(\nabla P^\alpha - \rho^\alpha g \right) \tag{4}$$

The total molar flux of the component $\mathrm{i} \in \mathrm{C}$ is denoted by $\boldsymbol{q_i}$ and the energy flux by $\boldsymbol{q_e}$, with

$$q_i = \sum_{\alpha \in \{\mathrm{g}, \mathrm{l}\}} C_i^\alpha \xi^\alpha V^\alpha, \quad q_e = \sum_{\alpha \in \{\mathrm{g}, \mathrm{l}\}} h^\alpha \xi^\alpha V^\alpha - \lambda \nabla T, \tag{5}$$

where λ stands for the bulk thermal conductivity of the fluid and rock mixture. The system of equations accounts for the molar conservation of each component $\mathrm{i} \in \mathrm{C}$ together with the energy conservation

$$\begin{aligned} &\phi(x) \partial_t n_i + div(q_i) = 0, \quad i \in C, \\ &\phi(x) \partial_t E + (1 - \phi(x)) \partial_t E_r + div(q_e) = 0. \end{aligned} \tag{6}$$

It is complemented by the following capillary relation between the two phase pressures and the pore volume balance

$$\begin{cases} P_c(S^g) = P^g - P^l, \\ \sum_{\alpha \in \{\mathrm{g}, \mathrm{l}\}} S^\alpha = 1. \end{cases} \tag{7}$$

Due to change of phase reactions assumed to be at equilibrium, phases can appear or disappear. Thanks to the extension of the phase molar fractions, the thermodynamic equilibrium can be expressed as the following complementary constraints for each phase $\alpha \in \{g, l\}$ combined with the equality of the gas and liquid fugacities of each component in the spirit of Lauser, Hager, Helmig and Wohlmuth (2011) and Masson, Trenty and Zhang (2014):

$$\begin{cases} S^\alpha \geq 0, \quad 1 - \sum_{i \in C} C_i^\alpha \geq 0, \quad S^\alpha (1 - \sum_{i \in C} C_i^\alpha) = 0, \quad \alpha \in \{\mathrm{g}, \mathrm{l}\}, \\ f_i^g(P^g, T, C^g) = f_i^l(P^l, T, C^l), \quad i \in C. \end{cases} \tag{8}$$

Note that our formulation of the model leads, independently on the set of present phases, to the fix sets of $2 \sharp C + 5$ unknowns and of $2 \sharp C + 5$ equations including the $\sharp C + 1$ conservation equations and the remaining $\sharp C + 4$ local closure laws.

2. SOIL-ATMOSPHERE BOUNDARY CONDITION FOR NON-ISOTHERMAL COMPOSITIONAL LIQUID GAS DARCY FLOW

The fluid and energy transport in high-energy geothermal systems is deeply governed by the conditions set at the boundary of the computational domain. In particular, it is well known that the modeling of the interaction between the porous medium model and the atmosphere plays an important role (refer to O'Sullivan, Pruess and Lippmann (2001)). In this section we propose a boundary condition model taking into account the convective molar and energy transfer and the vaporization of the liquid phase in the atmosphere as well as a liquid outflow condition.

2.1 Convective molar and energy transfer in the atmosphere

The convective molar transfer coefficient H_m and the convective energy transfer coefficient H_T account for the turbulent boundary layers of the gas flow and transport in the atmosphere. They are usually obtained from correlations used for environmental gas flows depending on the roughness of the soil surface including the effect of the vegetation, on the wind velocity, on the eddy diffusivity in the air stream and stability of the air above the heated soil surface. Let us also introduce the additional unknown $q^{g,atm}$ accounting for the gas molar flow rate at the interface on the atmosphere side oriented outward from the porous medium domain. The liquid phase is assumed to vaporize instantaneously when leaving the porous medium as long as the atmosphere is not saturated with water vapor. As soon as the atmosphere is vapor saturated at the interface, a liquid molar flow rate $q^{l,atm}$ is allowed to exit the porous medium. The prescribed far field atmospheric conditions are defined by the phase molar fractions $C_\infty^{\alpha,atm}, \alpha \in \{g,l\}$, the temperature T_∞^{atm} and the pressure P^{atm}, which fixes the far field atmospheric enthalpy of the water $h_{w,\infty}^{g,atm} = h_w^g(P^{atm}, T_\infty^{atm})$. The model assumes the continuity of the gas phase characterized by the continuity of the gas pressure $P^g = P^{atm}$, of the temperature T and of the gas molar fractions C^g at the interface. For any real u, let us set $(u)^+ = \max(0,u)$ and $(u)^- = \max(0,-u)$.

Thermodynamic equilibrium is always assumed at the interface in the sense that the gas molar fractions and pressure at the interface on the porous-medium side are extended by the one at equilibrium with the liquid phase in the absence of the gas phase. On the other hand, the liquid phase can appear or disappear according to the liquid phase complementary constraints. It results that the following equations hold at the interface:

$$
\begin{aligned}
&f_i^g(P^g,T,C^g) = f_i^l(P^l,T,C^l), \quad i \in C,\\
&\sum\nolimits_{i\in C} C_i^g = 1,\\
&S^l \geq 0, \quad 1 - \sum\nolimits_{i\in C} C_i^l \geq 0, \quad S^l(1 - \sum\nolimits_{i\in C} C_i^l) = 0,\\
&S^g = P_c^{-1}(P^g - P^l),\\
&S^g + S^l = 1,
\end{aligned}
\tag{9}
$$

where $P_c^{-1}(P^g - P^l)$ denotes the inverse of the monotone graph extension of the capillary pressure function $P_c(S^g)$.

At the interface, on the atmosphere side, the component gas molar normal flux and the gas energy normal flux are defined using the following two point fluxes between the interface on the atmosphere side and the far field atmospheric conditions at a given reference height:

$$
\begin{aligned}
q_i^{g,atm} &= (q^{g,atm})^+ C_i^g - (q^{g,atm})^- C_{i,\infty}^{g,atm} + H_m(C_i^g - C_{i,\infty}^{g,atm}), \quad i \in C,\\
q_e^{g,atm} &= (q^{g,atm})^+ h_w^g(P^g,T) - (q^{g,atm})^- h_{w,\infty}^{g,atm} + H_T(T - T_\infty^{atm}).
\end{aligned}
\tag{10}
$$

Regarding the interface energy balance, the model can also account for the solar and long wave radiation that is absorbed by and emitted from the soil surface defined by the following net radiation R_n $(W.m^{-2})$: $R_n = (1-a)R_s + R_a - \epsilon\sigma_{SB}T^4$, where R_a $(W.m^{-2})$ is the incoming long-wave radiation emitted by the atmosphere, R_s $(W.m^{-2})$ is the net short-wave radiation, a is the surface albedo, σ_{SB} $(W.m^{-2}.K^{-4})$ is the Stephan-Boltzman constant and ϵ the soil emissivity.

2.2 Liquid outflow complementary constraints

The liquid phase is assumed to vaporize instantaneously when leaving the porous medium as long as the atmosphere is not saturated with water vapor. As soon as the atmosphere is vapor saturated at the interface, the component molar and energy normal fluxes in the liquid phase defined by

$$
\begin{aligned}
q_i^{l,atm} &= C_i^{l,atm} q^{l,atm}, \quad i \in C,\\
q_e^{l,atm} &= h^l(P^l,T,C^{l,atm}) q^{l,atm},
\end{aligned}
\tag{11}
$$

are allowed to exit the porous medium, where $q^{l,atm} \geq 0$ is an additional unknown corresponding to the total liquid molar flow rate oriented positively outward to the porous-medium domain. We introduced the liquid molar fractions $C^{l,atm} = (C_i^{l,atm})_{i\in C}$ at the interface on the atmosphere side by the one at thermodynamic equilibrium with the gas phase, such that $f^l(P^{atm}, T, C^{l,atm}) = f^g(P^g, T, C^g)$. Note that, due to the jump of the capillary pressure which vanishes on the atmosphere side, $C^{l,atm}$ does not match in general with the liquid molar fractions on the porous-medium side C^l which satisfies $f^l(P^l, T, C^l) = f^g(P^g, T, C^g)$.

The liquid molar outflow rate $q^{l,atm}$ is determined by the following complementary constraints accounting for the thermodynamic equilibrium between the liquid and gas phases at the interface on the atmosphere side:

$$\begin{cases} 1-\sum_{i\in C} C_i^{l,atm} \geq 0, \quad q^{l,atm} \geq 0, \\ (1-\sum_{i\in C} C_i^{l,atm}) q^{l,atm} = 0. \end{cases} \tag{12}$$

It remains to eliminate the liquid molar fractions $C^{l,atm}$ from (11) and (12). Let us consider for $f \in \mathbb{R}^C$ the function $\mathcal{C}^l(f, P^l, T) \in \mathbb{R}^C$ defined as the unique solution of the equation $f^l(P^l, T, C^l) = f$. From $f^g(P^g, T, C^g) = f^l(P^g, T, C^{l,atm}) = f^l(P^l, T, C^l) := \bar{f}$, it results that $C^{l,atm} = \mathcal{C}^l(\bar{f}, P^g, T)$. On the one hand, if $S^l > 0$, it follows that $1 - \sum_{i\in C} C_i^{l,atm} = \sum_{i\in C}(C_i^l - C_i^{l,atm}) = \sum_{i\in C}(\mathcal{C}_i^l(\bar{f}, P^l, T) - \mathcal{C}_i^l(\bar{f}, P^g, T))$. Following Masson, Trenty and Zhang (2014), since the function $\sum_{i\in C} \mathcal{C}_i^l(f, P, T)$ is strictly decreasing with respect to P, it results that the complementary constraints (12) is equivalent to

$$\begin{cases} P^g - P^l \geq 0, \quad q^{l,atm} \geq 0, \\ (P^g - P^l) q^{l,atm} = 0. \end{cases} \tag{13}$$

On the other hand, if $S^l = 0$ then one has $P^g - P^l = P_c(1) > 0$ and $\sum_{i\in C} C_i^{l,atm} < 1$. It results that both conditions (12) and (13) imply that $q^{l,atm} = 0$. Finally, let us remark that if (13) holds, the liquid outflow fluxes in (11) rewrite as follows:

$$\begin{aligned} q_i^{l,atm} &= C_i^l q^{l,atm}, \quad i \in C, \\ q_e^{l,atm} &= h^l(P^l, T, C^l) q^{l,atm}. \end{aligned} \tag{14}$$

The model also takes into account the following component molar and energy flow rates which represent the precipitation recharge

$$\begin{aligned} q_i^{l,rain} &= C_i^{l,rain} q^{l,rain}, \quad i \in C, \\ q_e^{l,rain} &= h^l(P^{atm}, T_\infty^{atm}, C^{l,rain}) q^{l,rain}, \end{aligned} \tag{15}$$

with the rain molar fractions denoted by $C^{l,rain} = (C_i^{l,rain})_{i\in C}$, a temperature assumed at equilibrium with the far field atmosphere and the rain molar enthalpy denoted by $h^{l,rain} = h^l(P^{atm}, T_\infty^{atm}, C^{l,rain})$.

2.3 Evaporation-outflow boundary condition

Both the liquid outflow and evaporation models are combined in a single boundary condition, assuming that the liquid does not accumulate at the surface. Gathering the equations (10), (9), (13), (14), (15) together with the component molar and energy balance equations, the evaporation-outflow boundary condition at the interface is defined by the sets of $2 \,\#\, C + 7$ unknowns

$$X_\Gamma = (q^{g,atm}, q^{l,atm}, P^\alpha, T, S^\alpha, C^\alpha, \alpha \in \{\mathrm{g}, \mathrm{l}\}), \tag{16}$$

and equations

$$\begin{aligned} & q_i \cdot n = (q^{g,atm})^+ C_i^g - (q^{g,atm})^- C_{i,\infty}^{g,atm} + H_m(C_i^g - C_{i,\infty}^{g,atm}) + C_i^l q^{l,atm} + C_i^{l,rain} q^{l,rain}, \quad i \in C, \\ & q_e \cdot n = (q^{g,atm})^+ h_w^g(P^g, T) - (q^{g,atm})^- h_{w,\infty}^{g,atm} + H_T(T - T_\infty^{atm}) - R_n + h^l(P^l, T, C^l) q^{l,atm} + h^{l,rain} q^{l,rain}, \\ & P^g = P^{g,atm}, \\ & S^g = P_c^{-1}(P^g - P^l), \\ & S^g + S^l = 1, \\ & \sum_{i\in C} C_i^g = 1, \\ & S^l \geq 0, \quad 1 - \sum_{i\in C} C_i^l \geq 0, \quad S^l(1 - \sum_{i\in C} C_i^l) = 0, \\ & f_i^g(P^g, T, C^g) = f_i^l(P^l, T, C^l), \quad i \in C, \\ & P^g - P^l \geq 0, \quad q^{l,atm} \geq 0, \quad (P^g - P^l) q^{l,atm} = 0. \end{aligned} \tag{17}$$

3. STUDY OF THE SOIL-ATMOSPHERE BOUNDARY CONDITION ON 2D GEOTHERMAL TEST CASES

In these test cases, the porous medium is homogeneous of porosity $\phi(\boldsymbol{x}) = 0.35$ and of isotropic permeability $\boldsymbol{\Lambda}(\boldsymbol{x}) = k \times I$ with $k = 1\ D$. The relative permeabilities are defined by $k_r^\alpha(S^\alpha) = (S^\alpha)^2$ for each phase $\alpha \in \{g, l\}$. The capillary pressure function is given by the Corey law (see Figure 1)

$$P_c(S^g) = \begin{cases} -b\ln(1-S^g), & if\ O \le S^g \le S_1, \\ -b\ln(1-S_1) + \dfrac{b}{1-S_1}(S^g - S_1), & if\ S_1 < S^g \le 1, \end{cases} \tag{18}$$

with $b = 2\ 10^5\ Pa$ and $S_1 = 0.99$. The capillary pressure is regularized for $S^g \in (S_1; 1]$ to allow for the disappearance of the liquid phase (see Figure 1). Since there is no entry capillary pressure (in the sense that $P_c(0) = 0$), the complementary constraints $\min(\mathrm{P_c(S^g)}, \mathrm{q^{l,atm}}) = 0$ are equivalent to $\min(S^g, \mathrm{q^{l,atm}}) = 0$.

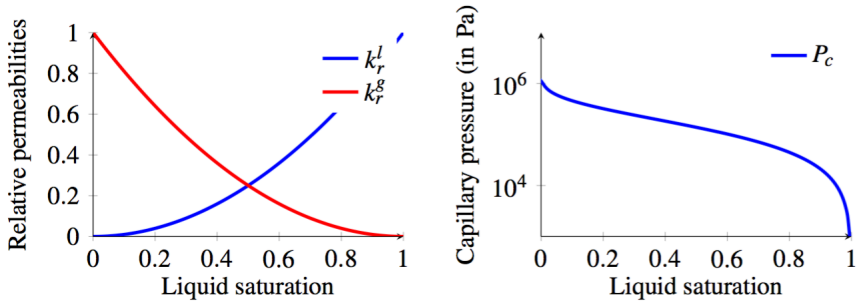

Figure 1: Relative permeabilities (left) of both phases $k_r^\alpha, \alpha = g, l$ and capillary pressure P_c (right) as functions of the liquid saturation S^l.

The gas thermodynamic laws are defined by the perfect gas molar density $\zeta^g = P^g/RT$, with $R = 8.314\ J.K^{-1}.mol^{-1}$ and the viscosity $\mu^g = (0.361\ T - 10.2\ 10^{-7}\ Pa.s$. The liquid molar enthalpy h^l and the gas molar enthalpies of each component h_a^g, h_w^g are taken from Schmidt (1969). The gas molar enthalpy is then defined by (1). The liquid molar density and viscosity are also from Schmidt (1969) and defined by $\zeta^l = (780.83795 + 1.62692\ \mathrm{T} - 3.06354\ \ 10^{-3}\ \mathrm{T}^2)(1 + 0.651\ \mathrm{C_s}) \times \frac{1}{0.018} mol.m^{-3}$, $\mu^l = (1 + 1.34\ \mathrm{C_s} + 6.12\ \mathrm{C_s^2})\ 10^{-3} \Big/ 0.02148(\mathrm{T} - 273 - 8.435 + \sqrt{8078.4 + (\mathrm{T} - 273 - 8.435)^2}\ ) - 1.2\ Pa.s$ with the salinity fixed to $\mathrm{C_s} = 35\ 10^{-3}\ Kg.Kg^{-1}$. The mass density is defined by $\rho^\alpha = \sum_{i \in C} C_i^\alpha m_i \zeta^\alpha, \propto \in \{g, l\}$ with the molar masses $m_a = 0.029$ and $m_w = 0.018\ Kg.mol^{-1}$. The vapour pressure $P_{sat}(T)$ is given by the Clausius-Clapeyron equation

$$P_{sat}(T) = 100\exp\left(46.784 - \frac{6435}{T} - 3.868\log(T)\right), \tag{19}$$

and the Henry constant of the air component is set to $H_a = 10^8 Pa$. The molar internal energy of each phase is considered to be equal to its enthalpy. The fugacities are defined by

$$\begin{cases} f_i^g = C_i^g P^g, \quad i = a, w, \\ f_w^l = C_w^l P_{sat}(T)\exp\left(-\dfrac{P_{sat}(T) - P^l}{1000RT/0.018}\right), \\ f_a^l = C_a^l H_a. \end{cases} \tag{20}$$

Finally, the thermal conductivity is fixed to $\lambda = 3\ \mathrm{W.m^{-2}}.K^{-1}$ and the rock energy per unit volume is given by $E_r(T) = 2\ 10^6\ T$ in $\mathrm{J.m^{-3}}$ with T in K.

The two dimensional test case illustrated in Figure 2 represents a simplified 2D cut of the Bouillante geothermal reservoir. It is run with two different upper boundary conditions to compare the solutions obtained with the evaporation-outflow boundary condition introduced in section 2 and with Dirichlet boundary conditions. The initial and left side conditions are defined by a pure water liquid phase ($S^l = 1$, $C_w^l = 1$) at hydrostatic pressure and by a linear temperature between the fixed top and bottom temperatures. The bottom boundary is impervious (no Darcy flux) with a fixed temperature of 400 K except in the interval $8000\ m \le x \le 1000\ m$ where a pure water liquid

input flux of $-2.9\ 10^{-2} mol.m^{-2}.s^{-1}$ at $550\ K$ is imposed. The right side of the domain is supposed thermally isolated (no Fourier flux) and impervious (no Darcy flux).

The top boundary conditions are test case dependent and are detailed below, except at the seabed boundary such that $z \leq 0\ m$, $x \leq 5000\ m$. The seabed boundary condition is defined by a pure water liquid phase ($S^l = 1$, $C_w^l = 1$) at hydrostatic pressure. The temperature is sea depth dependent. It is linear between the sea level $z = 0\ m$ at $300\ K$ and $z = -100\ m$ at $278\ K$, then constant below $z = -100\ m$.

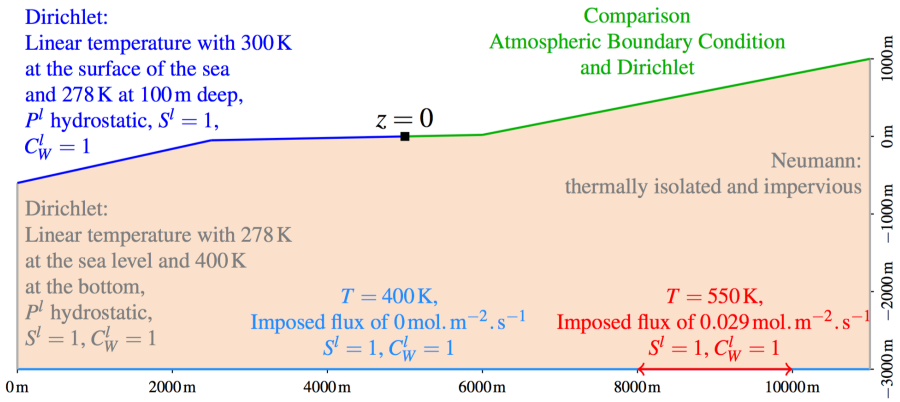

Figure 2: Illustration of the two dimensional domain and its boundary conditions.

A Voronoi mesh satisfying the admissibility condition of TPFA schemes at both inner and boundary faces has been generated. It contains approximately 3500 cells (around 4000 degrees of freedom) and is refined at the neighborhood of the top boundary with a volume ratio of 115 between the smallest and the largest cells of the mesh. The simulations are run over the time interval $(0, t_f), t_f =$ 1000 years, with an adaptive time stepping starting with an initial time step of 6 days in the Dirichlet case and of 1 day with the evaporation-outflow boundary condition. The maximum time step is fixed to 700 days in both cases.

3.1 2D geothermal test case with Dirichlet top boundary conditions

In this test case, the upper boundary is composed of three parts corresponding to the seabed ($z \leq 0\ m$ and $0 \leq x \leq 5000\ m$) described above, a sunny plain zone ($0 < z \leq 500\ m$ and $5000\ m < x \leq 8450\ m$) and a rainy mountain zone ($z > 500\ m$ and $8450 < x \leq 11000\ m$). The sunny plain zone is defined with the same parameters than the far field atmosphere conditions used in subsection 3.2 , which means that the relative humidity is fixed to 0.5, the temperature to $300\ K$ and the gas pressure to $P^g = 1\ atm$ from which we deduce that only the gas phase with water and air molar fractions $C_a^g = 0.99$, $C_w^g = 10^{-2}$ is present. The rainy mountain zone is characterized by a diphasic fluid at thermodynamic equilibrium which is fitted in such a way that the liquid flux entering the domain is similar to the one obtained in subsection 3.2 with the evaporation-outflow top boundary condition including the precipitation recharge. Then, using the simulation results of subsection 3.2 , the Dirichlet boundary condition for $z > 500\ m$ (which corresponds to $x > 8450\ m$) is defined by

$$\begin{cases} S^g = 0.72, & S^l = 0.28, \\ P^g = 1\ atm, & P^l = -153671\ Pa, \\ C_a^g = 0.97, & C_w^g = 0.03, \\ C_a^l = 10^{-3}, & C_w^l = 0.999, \\ T = 300\ K. \end{cases} \tag{21}$$

Figures 3 and 4 exhibit the temperature and the gas saturation in the reservoir at final time and Figure 5 shows the main physical variables at different times along the top cells. The top cells are chosen rather than the top boundary since the top boundary variables are fixed by the Dirichlet conditions. The degree of freedom of the top cell is the center of the cell which is located approximately $12\ m$ below the top boundary. Let us notice the sharp gradients observed in the plots of Figure 5 at the shoreline $x = 5000\ m$. From Figures 3, 4 and 5, let us remark that the high temperature flux goes out of the reservoir at the top boundary on both sides of the shoreline approximately in the interval $3575\ m \leq x \leq 5550\ m$. Inside this interval, we can observe a temperature drop in the interval $4800\ m \leq x \leq 5200\ m$. It is explained by the evaporation of the liquid phase which cools down the surface neighborhood.

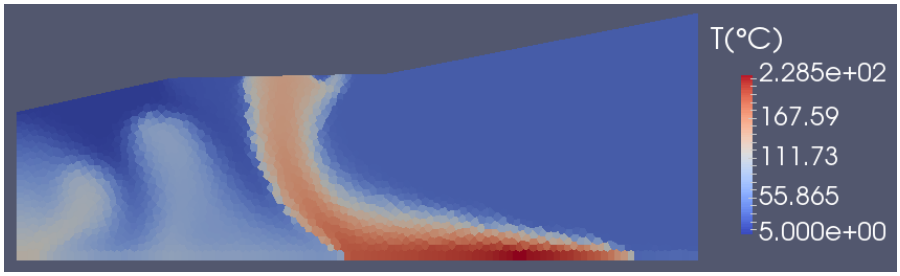

Figure 3: Temperature (in Celsius) at final time (1000 years) obtained with the Dirichlet top boundary conditions.

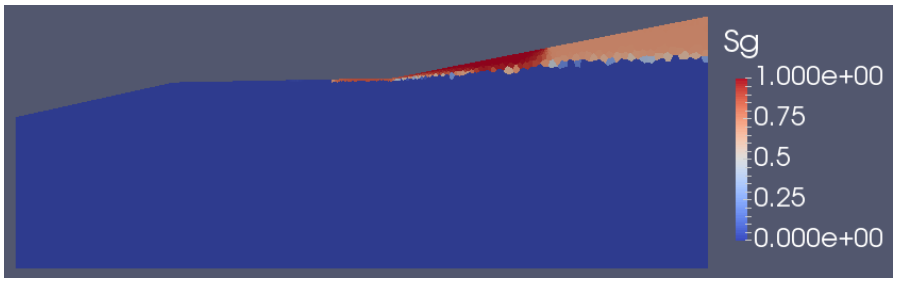

Figure 4: Gas saturation at final time (1000 years) obtained with the Dirichlet top boundary conditions.

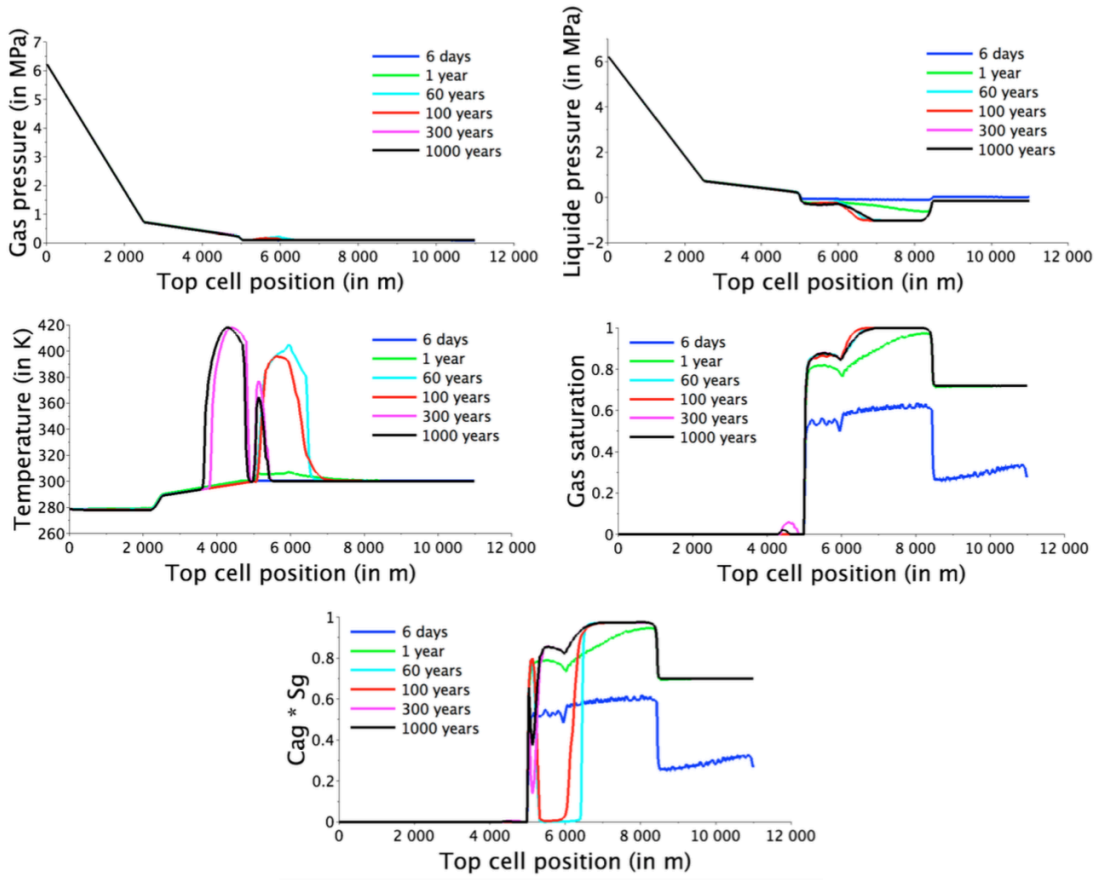

Figure 5: Gas and liquid pressures (in MPa), temperature (in K), gas saturation and air molar fraction in the gas phase weighted by the gas saturation obtained at times t = 6 days, 1 year and 60, 100, 300, 1000 years along the top cells using the Dirichlet top boundary condition.

3.2 2D geothermal test case with the soil-atmosphere evaporation-outflow boundary condition

In this subsection, the Dirichlet conditions on the sunny plain and rainy mountain zones are replaced by the evaporation-outflow boundary condition developed in section 2. The short and long wave radiation coming from the atmosphere and reaching the soil surface is fixed to $(1-a)R_s + R_a = 340\ W.m^{-2}$ and the soil emissivity to $\varepsilon = 0.97$. The convective molar and energy transfer coefficients are set to $H_m = 0.69\ mol.m^{-2}.s^{-1}$ and $H_T = 29{\times}H_m = 20\ W.m^{-2}.K^{-1}$. The far field atmospheric conditions are set to $C_{a,\infty}^{g,atm} = 0.99$, $C_{w,\infty}^{g,atm} = 10^{-2}$, $T^{atm} = 300\ K$ and $P^{atm} = 1\ atm$, corresponding to a relative humidity of 0.5. The precipitation recharge is null on the sunny plain zone and fixed to $q^{l,rain} = -3.2\ 10^{-2}\ mol.m^{-2}.s^{-1}$on the rainy mountain zone with $C_w^{l,rain} = 0.999$ and $C_a^{l,rain} = 10^{-3}$. This precipitation recharge corresponds to roughly twice the observed rainfall of 9 m in 2016. It has been doubled since the reservoir 2D cut is assumed to be along a fault plane which favors the water intrusion.

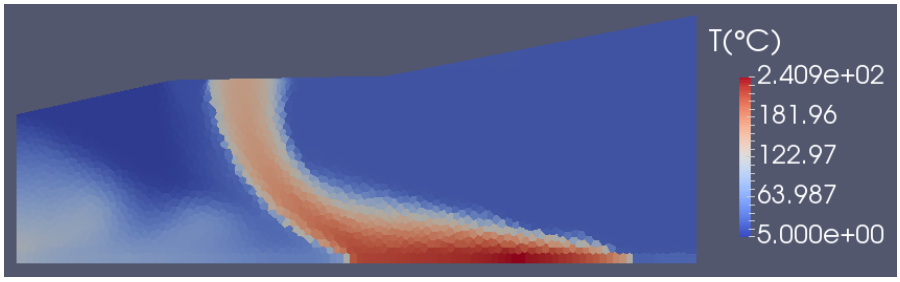

Figure 6: Temperature (in Celsius) at final time (1000 years) obtained with the evaporation-outflow boundary condition.

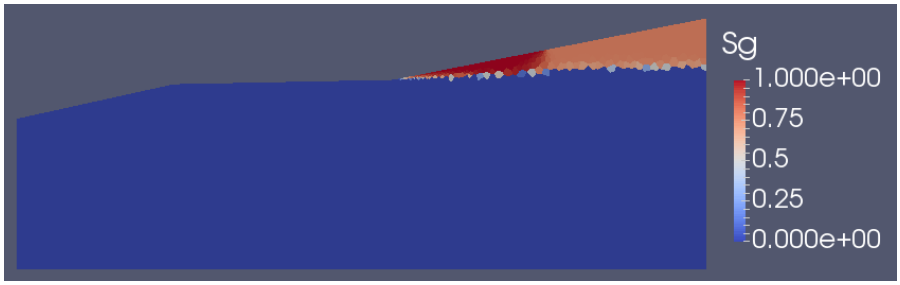

Figure 7: Gas saturation at final time (1000 years) obtained with the evaporation-outflow boundary condition.

Figures 6 and 7 exhibit the temperature and the gas saturation in the whole domain at final time. Figure 8 plots the main physical variables along the top boundary while Figure 9 plots the same variables along the top cells to be compared with the above Dirichlet test case.

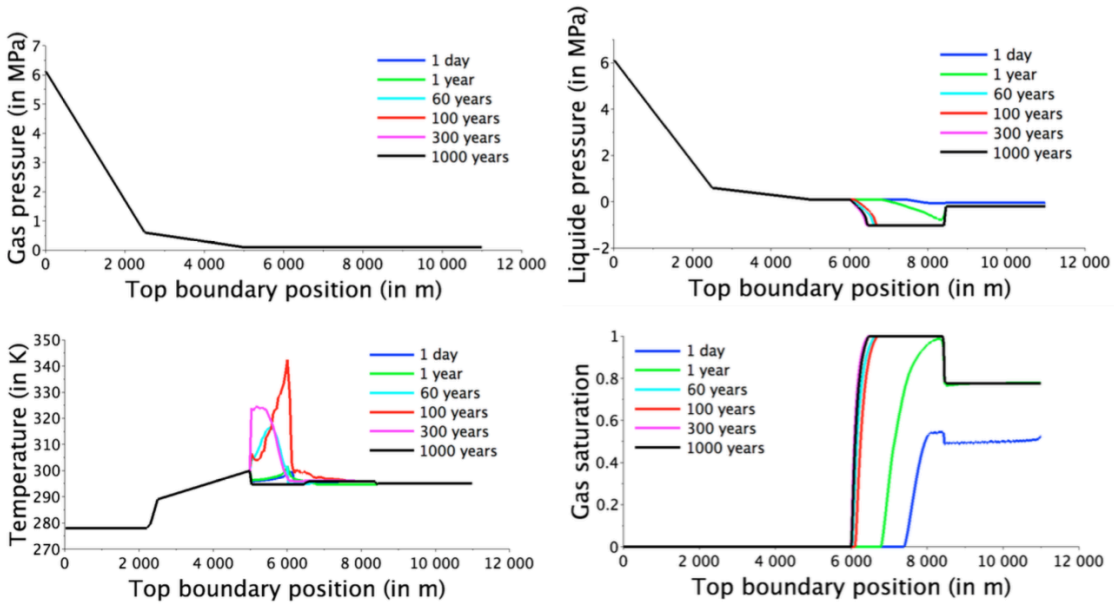

Figure 8: Gas and liquid pressures (in MPa), temperature (in K) and gas saturation obtained at times t = 1 day, 1 year and 60, 100, 300, 1000 years at the top boundary using the evaporation-outflow boundary condition.

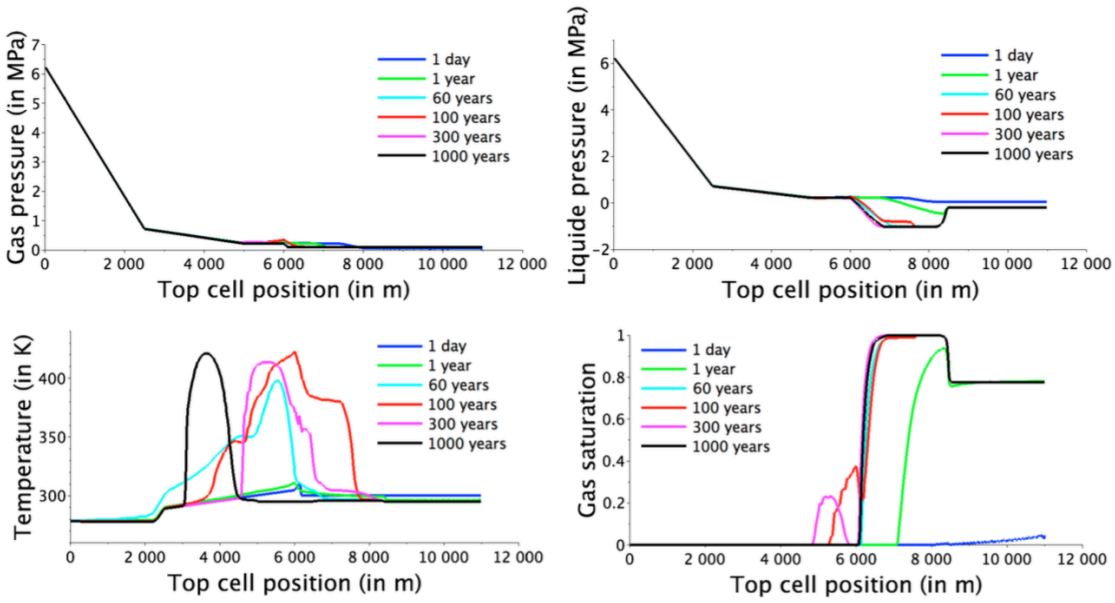

Figure 9: Gas and liquid pressures (in MPa), temperature (in K) and gas saturation obtained at times t = 1 day, 1 year and 60, 100, 300, 1000 years at the top cells using the evaporation-outflow boundary condition.

Figures 6**,** 7, when compared with Figures 3**,** 4, show that at final time the evaporation-outflow boundary condition shifts the high temperature zone to the left, from $3575\ m \leq x \leq 5550\ m$ at the top boundary for the Dirichlet boundary condition to $2950\ m \leq x \leq 4575\ m$ for the evaporation-outflow boundary condition. This shift can be explained by the lower liquid pressure $P^l = P^{atm} - P_c(1)$ provided at the top boundary by the gas Dirichlet condition than the one provided by the evaporation-outflow boundary condition with in particular $P^l = P^g = P^{atm}$ between say $x \leq 5000\ m$ and $x \leq 6000\ m$ as a result of the liquid outflow. It also results that the temperature drop near the shoreline does no longer appear. The gas saturation remains null below the seabed and the desaturated zone is shifted to $x > 5000\ m$ (see also Figures 5 and 9). It can also be noticed that the desaturated zone is deeper with the evaporation-outflow than with the Dirichlet boundary condition.

In both Figures 3**,** 4 and 6**,** 7, convective thermal instabilities can be noticed which are induced artificially by the left Dirichlet boundary conditions. An efficient way to get rid off these artefacts is to model the seawater intrusion taking into account the additional salt component and the dependence of the liquid viscosity and mass density on the salinity. This is the object of the next test case.

3.3 2D geothermal test case with a water-air-salt thermodynamic system

In this subsection, the previous test case of subsection 3.2 is extended to take into account the dissolution of the salt component denoted by s in the liquid phase. Since our model assumes all components to be present in both phases, the liquid and gas phases are now a mixture of three components, the water denoted by w, the air denoted by a and the salt denoted by s, setting $\mathcal{C} = \{w, a, s\}$. The liquid molar density ζ^l and viscosity μ^l are functions of the salinity C_s in $Kg.Kg^{-1}$ which is now related to the liquid molar fractions by $C_s = \frac{C_s^l m_s}{\sum_{i \in \mathcal{C}} C_i^l m_i}$, with $m_s = 58.44\ \ 10^{-3}$, $m_w = 18\ \ 10^{-3}$, $m_a = 29\ \ 10^{-3}\ Kg.mol^{-1}$. The air and water fugacities in both phases are still given by (20) and the fugacities of the salt component are defined by

$$\begin{cases} f_s^g = C_s^g P^g, \\ f_s^l = C_s^l H_s, \end{cases} \tag{22}$$

with a very low Henry constant $H_s = 10^{-1}\ Pa$ in order to keep the vaporization of the salt component in the gas phase negligible. The Dirichlet boundary condition at the interface between the sea and the reservoir now uses the input salinity $C_s = 35\ \ 10^{-3} Kg.Kg^{-1}$ of the sea water. The input salinity at the left side of the reservoir as well as at the bottom boundary is fixed to the lower value $C_s = 20\ \ 10^{-3} Kg.Kg^{-1}$. The remaining boundary and initial conditions are unchanged compared with the previous test case, using a zero salinity for the initial water in the reservoir and for the precipitation recharge.

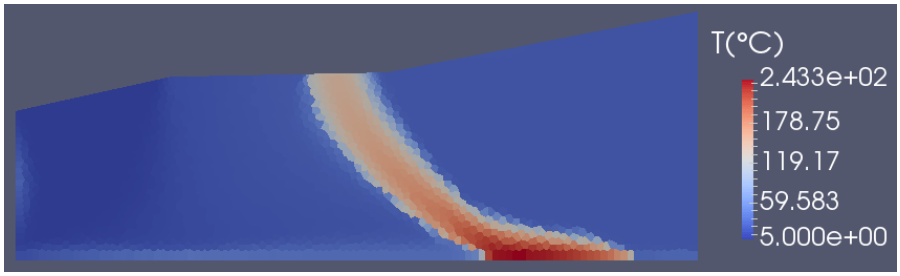

Figure 10: Temperature (in Celsius) at final time (1000 years) obtained with the air-water-salt test case.

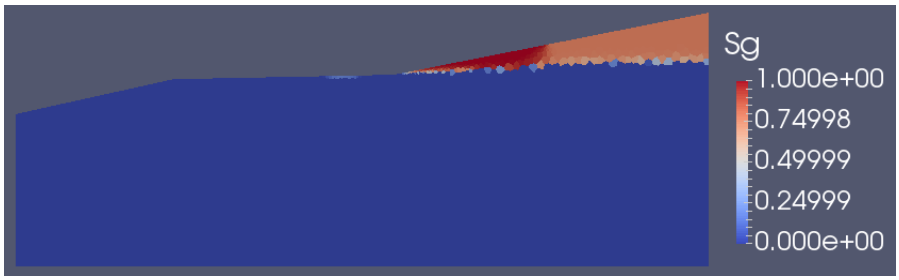

Figure 11: Gas saturation at final time (1000 years) obtained with the air-water-salt test case.

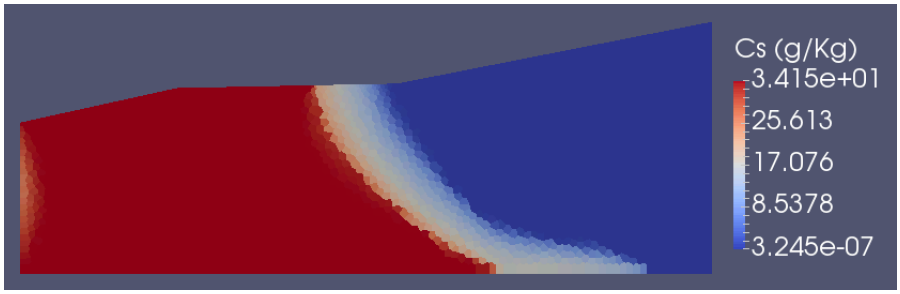

Figure 12: Salinity of the liquid phase (in $g.Kg^{-1}$) at final time (1000 years) obtained with the air-water-salt test case.

Figures 10**,** 11**,** 12 exhibit the temperature, the gas saturation and the salt mass fraction in the liquid phase in the reservoir at final time. Figures 13 and 14 show the physical variables at the top boundary and along the top cells.

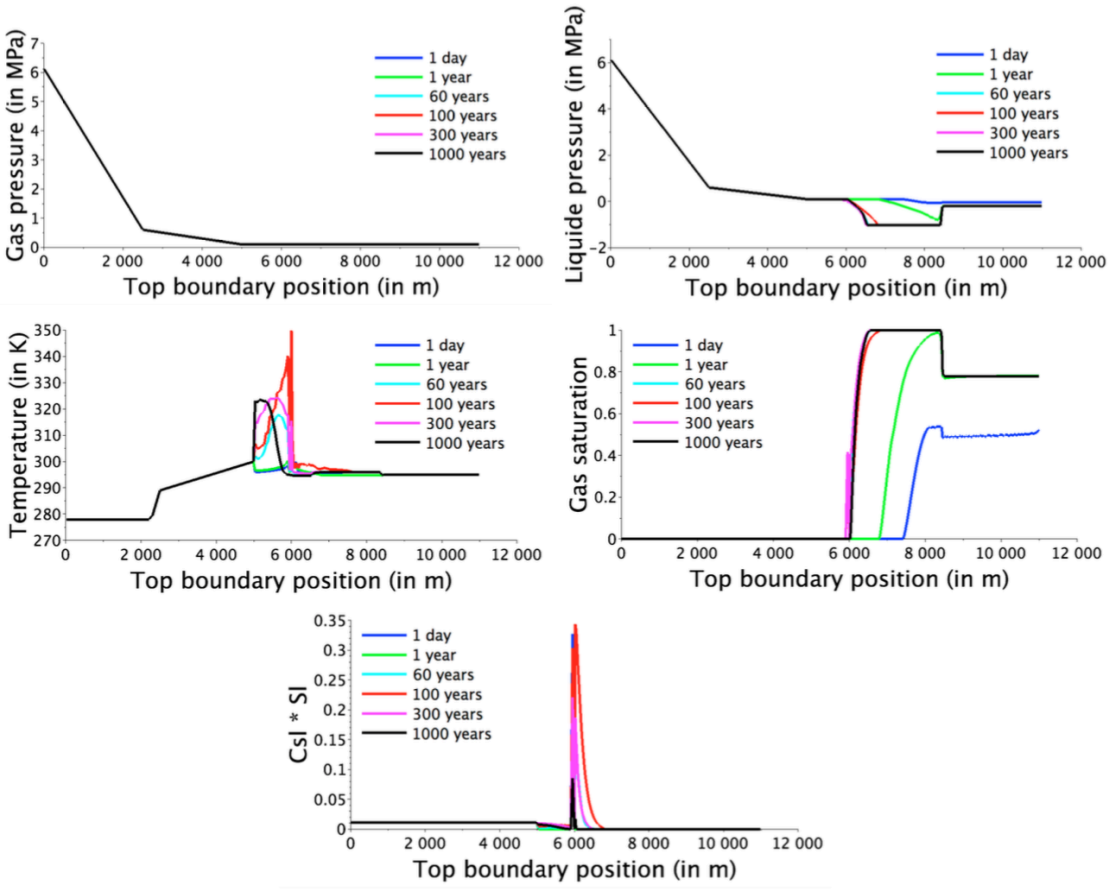

Figure 13: Gas and liquid pressures (in MPa), temperature (in K), gas saturation and salt molar fraction in the liquid phase weighted by the liquid saturation at times t = 1 day, 1 year and 60, 100, 300, 1000 years at the top boundary, obtained with the air-water-salt test case.

It is clear from the comparison between Figures 10, 11, 12 and Figures 3, 4 and 6, 7 that the sea water intrusion prevents as expected the development of the convective thermal instabilities from the left side of the reservoir. This is due to the higher salinity of the seawater compared with the left side and bottom salinity. It also explains why the high temperature zone is shifted to the right in this test case compared with the previous test case. The plot of the salt molar fraction in the liquid phase at final time in Figures 10, 11, 12 clearly shows that the reservoir is splitted in 3 zones depending on the source of the water flux, the sea water zone on the left, the rain water zone on the right and the high temperature water zone in between. A high salt molar fraction in the liquid phase can also be noticed in Figure 13 at the top boundary due to the liquid vaporization. It goes up to 0.35 at time t =100 years and then decreases to 0.1 at final time. It could induce the precipitation of the salt not taken into account in our model.

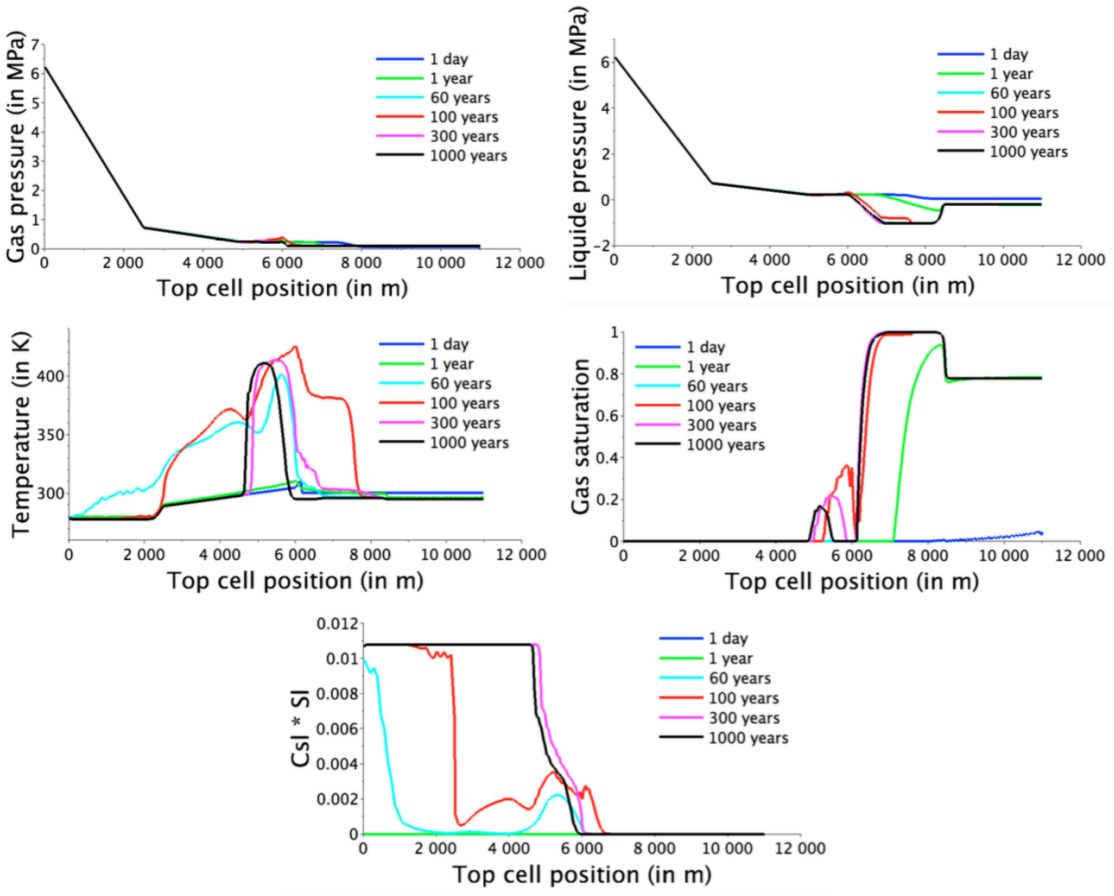

Figure 14: Gas and liquid pressures (in MPa), temperature (in K), gas saturation and salt molar fraction in the liquid phase weighted by the liquid saturation at times t = 1 day, 1 year and 60, 100, 300, 1000 years along the top cells obtained with the air-water-salt test case.

4. CONCLUSION

In this work, a new formulation for non-isothermal compositional gas liquid Darcy flows based on natural variables and using extended phase molar fractions has been introduced. The non-isothermal compositional model is coupled with an advanced soil-atmosphere boundary condition accounting for the vaporization of the liquid phase in the atmosphere, the convective molar and energy transfer, a liquid outflow condition as well as the precipitation recharge and the radiation. The efficiency of the formulation and the soil-atmosphere evaporation-outflow boundary condition have been studied on several 2D test cases of a 2D cut of the Bouillante high energy geothermal field in Guadeloupe with both air-water and air-water-salt thermodynamic systems. The importance for geothermal simulations of the top boundary condition taking into account the seabed, the sunny plain and the rainy mountain zones is enlightened by comparison with a fitted Dirichlet boundary condition.

REFERENCES

Ben Gharbia, I. and Jaffré, J.: Gas phase appearance and disappearance as a problem with complementarity constraints, *Mathematics and Computers in Simulation*, (2013).

Class, H. and Helmig, R. and Bastian, P.: Numerical simulation of non-isothermal multiphase multicomponent processes in porous media: 1. An efficient solution technique, *Advances in Water Resources*, **25**, (2002), 533-550.

Lauser, A. and Hager, C. and Helmig, R. and Wohlmuth, B.: A new approach for phase transitions in miscible multi-phase flow in porous media, *Advances in Water Resources*, **34**, (2011), 957-966.

Masson, R. and Trenty, L. and Zhang, Y.: Formulations of two phase liquid gas compositional Darcy flows with phase transitions, *International Journal on Finite Volumes*, **11**, (2014).

O'Sullivan, M. J. and Pruess, K. and Lippmann, M. J.: Geothermal reservoir simulation: the state-of-practice and emerging trends, *Geothermics*, **30**, (2001), 395-429.

Schmidt , E: Properties of water and steam in S.I. units, Springer-Verlag, (1969).